

No. 69 WAVELENGTH DEPENDENCE OF POLARIZATION, IV:
VOLCANIC CINDERS AND PARTICLES*

by DAVID L. COFFEEN

December 29, 1964

ABSTRACT

Five laboratory samples were measured for comparison with the moon, using a Wollaston photopolarimeter with filters near 0.36, 0.53, and 0.97 μ , having the sun as light source. Three of the samples were porous dust layers of ground volcanic cinder particles smaller than 37 μ , in "fairy-castle" structures. The other two were: a porous but solid lava fragment, and the same fragment covered with a fairy-castle dust layer made from the same lava. The solid lava fragment is more highly polarized than the moon, and has essentially no wavelength dependence. The wavelength and phase dependence of the lunar polarization is closely matched by the fairy-castle structures. No dependence of polarization on sample orientation was found for the volcanic materials. Differential photometry was done with the same filters using a smoked MgO layer as comparison. All samples show a linear brightness increase (in magnitudes) from 50° to 20° phase, similar to the moon. The fairy-castle structures show an appreciable opposition effect in the ultraviolet which, however, almost disappears in the green and infrared.

PAPER III (Gehrels *et al.* 1964) shows the wavelength dependence of polarization and of brightness for selected lunar regions. Recent laboratory work was done by Hapke and Van Horn (1963) on samples of loosely compacted dust particles, referred to as "fairy-castle" structures. However, Hapke and Van Horn have as yet not used the wavelength dependence of polarization nor has accurate photometry of lunar regions near zero phase been available to them. Therefore, the present paper uses in the laboratory the equipment of Paper III in order to observe brightness and polarization with ultraviolet, green, and infrared filters and at a range of phases as was done for the lunar regions.

I. Equipment

a. Laboratory Arrangement

The apparatus consisted of a coelostat, a tube for the light path into the room, a sample mount, and the Wollaston photometer. The apparatus was arranged with a horizontal plane of vision (defined by the tube axis, the sample, and the photometer). Large optical paths (about 6 ft) from tube end to sample and from sample to photometer were used to permit measurements as near zero phase as possible. The photometer was mounted horizontally, and on wheels in order to vary the phase angle (defined as the angle at the sample, between the direction to the light source and the direction to the photometer).

b. Zero-Phase Arrangement

At zero phase angle the photometer would ordinarily eclipse the light source. Therefore zero-phase photometry was done with the incoming beam passing straight through a thin inclined glass plate, the light reflected by the sample being observed at the 90° reflection by the glass plate. No corrections for the several reflections were necessary as the photometry was made differentially using a comparison plate, as described in Sec. IV.

c. Light Source

For realistic comparison of laboratory data with lunar measurements the illumination of the sample should resemble the illumination of the moon by the sun. In particular, the source must have a high intensity from about 3300 to 10 000 Å (for precise UGI photometry of low-albedo samples) similar to the solar energy distribution, it must be reasonably well collimated (light directly from the sun converges from only about 0°5), it must produce a minimum of stray light in the laboratory, and it must have broad-band polychromatic radiation or the polarimeter's Lyot depolarizer will not function properly. An artificial source with both spectral continuity and sufficient intensity in the ultraviolet was not found, and a coelostat for solar illumination was used instead. The reflection of the sun from the coelostat's two front-surfaced aluminized mirrors was directed horizontally through the 15-ft long hollow tube of 6 in. diameter, painted flat black inside, which was mounted through a hole in the laboratory door. The direction of the incoming beam was maintained within ± 0.3 by readjustments of the motorized coelostat. The polarization introduced by the reflections from the two mirrors was eliminated by placing a 1-in.-diameter Lyot depolarizer at the end of the tube.

d. Sample Mount

The sample required a support which would permit at each phase angle a wide range of orientations. A modified theodolite was used as mount so that the phases and orientations could be precisely determined. Translation of the sample mount in three orthogonal directions was necessary in order to maintain observation of a given point, regardless of the orientation of the sample.

e. Diaphragms

In place of a telescope a 1-in.-diam. lens, of 7 in. focal length, was installed to focus the sample on the photometer diaphragm. The fairy-castle structures were usually

*Reprinted from the *Astronomical Journal*, Vol. 70, No. 6, pp. 403-413, August 1965, with permission.

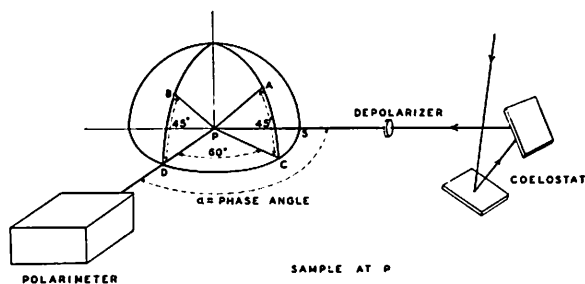


FIG. 1. Laboratory arrangement. Points *A*, *B*, *C*, and *D* represent four orientations of the sample normal, for a given phase angle α .

measured with the smallest diaphragm. The solid-lava fragment had to be measured with two larger diaphragms because of its irregularities in shape. The angular widths of the acceptance cones (and the corresponding spot diameters on the samples) are: 12'2 (0.71 cm); 18'6 (1.08 cm); and 26'8 (1.56 cm). All measurements on the solid fragment were of the same region on the sample, but this was not even attempted with fairy-castle layers as they are homogeneous in composition and structure, on a scale of several millimeters.

f. Effective Wavelengths

The same Wollaston photometer, filters, and ice-boxes of Gehrels and Teska (1960, 1963) were employed. The RCA 7102 icebox was used with both the Infrared and Green filters, while the EMI 6255S icebox was used with both Green and Ultraviolet filters. The effective wavelengths as defined by

$$\lambda_{\text{eff}} = \int \lambda S(\lambda) T(\lambda) d\lambda / \int S(\lambda) T(\lambda) d\lambda$$

were calculated by numerical integration using values of tube sensitivity $S(\lambda)$ published by RCA and EMI, and filter transmission $T(\lambda)$ determined by Pellicori.

Table I gives the effective wavelengths for the various combinations of filters and tubes, assuming incident light of equal intensity at all wavelengths. These values are in error if there exist differences between the published sensitivity curves and the sensitivities of the particular tubes used. Furthermore the effective wavelength depends upon the spectral distribution of the incident light, and so will differ for each sample measured.

TABLE I. Effective wavelengths.

Filter	Tube	λ_{eff} μ	$1/\lambda_{\text{eff}}$ μ^{-1}
<i>I</i>	RCA7102	0.97	1.03
<i>G_i</i>	RCA7102	0.54	1.85
<i>G_u</i>	EMI6255S	0.51	1.95
<i>U</i>	EMI6255S	0.36	2.78

2. Samples

Lyot (1929) found that certain volcanic ash powders exhibit almost exactly the lunar polarimetric phase function in the visual region.

Hapke and Van Horn (1963) found that dielectric particles less than about 15 μ in diameter will bond together (when sifted onto a surface) to form a very porous structure with interconnected openings, which they term "fairy-castle" structure. The particles may be dropped from any height if in atmosphere, since collisions with air molecules establish a constant terminal velocity which is low enough so that the fairy-castle structure may be built up (presumably by van der Waals bonding). But in vacuum the maximum distance of fall is about 1 mm on the earth; greater heights result in disruption of the structure and consequent "gravel pile" packing (Hapke and Van Horn 1963).

Three types of volcanic cinders were collected by A. Herring near the top of the Haleakala Crater, Maui, Hawaii. I am indebted to Mr. Herring and to Dr. G. P. Kuiper for providing me with the laboratory samples. No mineralogical or chemical analyses have been performed on the samples, but they have the following characteristics:

Type number	Average particle size	Visual color
1	0.1 mm	reddish brown
2	3 mm	tan
3	3 mm	gray

Fairy-castle layers of the volcanic cinders were deposited on wet, flat black paint (to provide bonding of particles and surface) on 3-in. square plates of aluminum. The cinders had been ground by hand with mortar and pestle and sifted through a 400-mesh sieve (maximum hole size 37 μ) held about 6 in. above the aluminum plate. The fairy-castle layers were not disturbed by repeated inclining at 45°, but they could not be inverted without damage. The low bulk density of the layers is observable with a microscope and is evidenced by the fact that a layer collapses when subjected to a hard shock.

A 3-in.-long brown Hawaiian lava fragment was sawed in half and the cut surface was measured photometrically and polarimetrically, both with and without a fairy-castle covering made from the other half. The solid fragment itself is very porous, but its cavities are not generally interconnected.

Two other fairy-castle layers (one of crushed charcoal and the other of instant-tea particles) having particle diameters less than 37 μ were measured to investigate the dependence of the polarization of fairy-castle layers on the properties of their individual particles.

3. Polarimetry

The polarization measurements with the Wollaston photometer followed the procedure described by

Gehrels and Teska (1960). Each determination involved, at each of six Wollaston prism orientations, a measurement with and without a Lyot depolarizer in the photometer beam. The least-squares cosine-curve fits (to determine the amplitude and orientation of plane polarization) were done with the IBM 7090 at the Western Data Processing Center in Los Angeles.

Table II gives the polarization observations. The sample orientations are described in Sec. III B, below; P is the percentage plane polarization of the reflected light; θ_r is the angle between the normal to the plane of vision and the direction of the electric vector maximum (P , θ_r , and the phase angle are as used in Paper III); the date of measurement is given in the last column.

a. Quality of Measurements

The mean residual between the observed values and the least-squares cosine-curve is ± 0.0028 mag., which gives a probable error of the published result of $\pm 0.06\%$ polarization. Colons are used in the table when the mean residual of the least-squares solution is greater than three times the average.

But the scatter of repeated measurements does not confirm this probable error of $\pm 0.06\%$. In several cases the repetitions differ by less than 0.06% , but in some cases they differ by as much as 1.5% . This suggested that an extraneous source of polarization is included in the measurements.

The source of additional error in the polarization was investigated with a relatively unpolarized ($< 2\%$) 150-W slide projector used, without a depolarizer, as the light source on 9 September (Table II). Secondly, a smoked MgO plate was measured with solar illumination, with the depolarizer in the incident beam, as usual. The two methods of illumination give good agreement for fairy-castle No. 3, but 11° and 17° phase measurements of the solid lava fragment (Table II) show a consistent ratio between the lamp and solar P values of about 1:4. The observations on the magnesium oxide plate are inconclusive; in this case there appears to be a strong dependence of P on sample orientation. The MgO plate apparently introduces several percent polarization at 90° phase and therefore could not serve as a nonpolarizing standard. However, the dependence of polarization on the light source led to discovery that the two depolarizers (which are both in the light beam during half the number of integrations) can transmit partial polarization of the incident beam.

The polarization introduced by the pair of aluminized coelostat mirrors depends on the geometry of the mirrors and therefore on the time of day, declination of the sun, and terrestrial latitude. In a similar situation Bumba and Topolová-Růžičková (1962) found the polarization to decrease with increasing altitude of the sun, reaching a minimum of about $\frac{1}{2}\%$ when the sun is in the meridian; the polarization approaches 6% at sunrise and sunset, but is less than 2% between three

hours after sunrise and three hours before sunset (during which interval the present measurements were made). In the laboratory two depolarizers in series are found to transmit (depending on their relative orientation) from less than 1% to about 30% of incident polarization, whereas a single depolarizer transmits less than 1% . Thus systematic errors of at most 1% could be present in P .

The average of all θ_r values which are obviously nearer 90° than 180° is 88.8 . For phase angles greater than 25° , the average of all θ_r values which are nearer 180° than 90° , is 179.7 . The additional polarization from the incident beam probably enters into the θ_r , average in a random fashion since during the course of measurements the depolarizer in the incoming beam was removed several times, being replaced in a presumably different orientation each time. The incident polarization precludes a detailed investigation of variation of θ_r with phase angle since the amount of sample polarization and therefore the relative importance of the incident polarization varies with phase. But it is noted that the average θ_r 's agree well with the lunar observations in that all plane polarization seems to be either in the plane of vision or perpendicular to it, depending on the phase.

Instrumental polarization was not measured for lack of a suitable unpolarized source; it may have caused errors of the order of $\pm 0.11\%$ (Gehrels and Teska 1963). The instrumental depolarization was not determined as it is negligible compared to the systematic errors; according to Paper III (p. 828) the values of P in Table II should have been multiplied by 1.004.

In future laboratory work the depolarizer interaction should, of course, be eliminated. It appears that this can be done simply by removing the depolarizer from the light-source tube whenever the other depolarizer is in the polarimeter, and using the light-source depolarizer on the alternate measurements when the polarimeter depolarizer is out of the beam. In this manner, any instrumental polarization in the incoming beam cannot reach the Wollaston prism, yet the light never passes through more than a single depolarizer.

b. Orientation of the Sample

In order to simulate a region on the lunar surface it was necessary to maintain the sample at a fixed orientation relative to the polarimeter while varying the phase angle and therefore also the angle of incidence. The fragility of the fairy-castle structures prevented their measurement perpendicular to the polarimeter (i.e., suspended in a vertical plane). It was also desired to measure the samples at more than one orientation to check for variation of polarization with orientation, independent of the phase angle. Polarimetry of the fairy-castle structures was therefore done for two sample orientations, A and B , having azimuthal inclinations to the polarimeter of 60° and 0° , respectively, both at 45°

TABLE II (continued)

Sample	Phase	Filter ^a	Orien- tation ^b	<i>P</i>	θ_r	Date 1963	Sample	Phase	Filter ^a	Orien- tation ^b	<i>P</i>	θ_r	Date 1963	
Solid lava fragment	50°0	<i>U</i>	<i>D</i>	16.1%	179°	9/6	Solid lava frag- ment overlaid by its fairy- castle dust layer	50°0	<i>U</i>	<i>A</i>	9.4%	181°	9/12	
		<i>G_u</i>	<i>B</i>	14.0	180	9/9			<i>U</i>	<i>B</i>	9.2	181	9/12	
		<i>G_u</i>	<i>D</i>	14.4	180	9/6			<i>G_u</i>	<i>A</i>	8.2	180	9/12	
		<i>G_u</i>	<i>D</i>	14.7	179	9/9			<i>G_u</i>	<i>B</i>	7.9	181	9/12	
		<i>I</i>	<i>C?</i>	15.5	183	9/7			<i>I</i>	<i>A</i>	8.2	182	9/15	
	90.0	<i>I</i>	<i>D?</i>	15.4	182	9/7		90.0	<i>U</i>	<i>A</i>	20.5	179	9/12	
		<i>U</i>	<i>A</i>	51.4	180	9/8			<i>U</i>	<i>A</i>	26.7	181	9/15	
		<i>U</i>	<i>C</i>	54.1	180	9/6			<i>G_u</i>	<i>A</i>	16.8	179	9/12	
		<i>G_u</i>	<i>C</i>	51.4	180	9/6			<i>I</i>	<i>A</i>	20.1	180	9/15	
		<i>G_i</i>	<i>C?</i>	48.5:	180	9/7			110.0	<i>U</i>	<i>A</i>	20.7	178	9/12
	<i>I</i>	<i>C?</i>	52.8:	180	9/7	<i>G_u</i>		<i>A</i>		16.1	178	9/12		
	110.0	<i>U</i>	<i>C</i>	68.1	180	9/6		135.0		<i>U</i>	<i>A</i>	16.2	175	9/12
		<i>G_u</i>	<i>C</i>	67.6:	180	9/6				<i>G_u</i>	<i>A</i>	13.7	173	9/12
		<i>I</i>	<i>C?</i>	70.7:	180	9/7				Smoked MgO plate	11.0	<i>U</i>	<i>B</i>	0.9
	135.0	<i>U</i>	<i>C</i>	60.6	179	9/6		<i>U</i>	<i>D</i>			0.3	51	9/9
<i>G_u</i>		<i>C</i>	62.4	179	9/6	<i>G_u</i>	<i>B</i>	1.4	7			9/9		
<i>I</i>		<i>C?</i>	64.0	180	9/7	<i>G_u</i>	<i>D</i>	0.1	57			9/9		
Solid lava frag- ment overlaid by its fairy- castle dust layer	11.0	<i>U</i>	<i>B</i>	1.4	65	9/12	<i>G_u</i>	<i>F</i>	0.2			65	9/9	
		<i>G_u</i>	<i>B</i>	1.3	76	9/12	50.0	<i>U</i>	<i>B</i>	4.5	187	9/9		
	17.0	<i>U</i>	<i>B</i>	1.1	50	9/12		<i>U</i>	<i>D</i>	2.5	184	9/9		
		<i>G_u</i>	<i>B</i>	0.6	63	9/12		<i>G_u</i>	<i>B</i>	5.7	186	9/9		
	25.0	<i>U</i>	<i>B</i>	1.5	192	9/12		<i>G_u</i>	<i>D</i>	2.9	182	9/9		
		<i>G_u</i>	<i>B</i>	1.3	185	9/12								

^a The filters are described in Table I.
^b Sample orientations are described in Sec. III B.
^c A different (cleaner) secondary mirror was used in the coelostat.
^d *P* and θ_r are averages from two independent sets of reductions of the same data; the greatest differences were 0.06% and 1°3.
^e A tungsten source (150-W slide projector) was used instead of sunlight and coelostat.

elevation of the sample-normal above the plane of vision (Fig. 1). The solid lava fragment was also measured with the sample normal *in* the plane of vision—orientations *C* and *D* with azimuthal inclinations of 60° and 0°, respectively, both at 0° elevation. These four orientations result in various angles of incidence, depending on the phase angle, as shown in Table III. The angles of emergence for orientations *A*, *B*, *C*, and *D* are, respectively, 69°3, 45°0, 60°0, and 0°0. All values are believed correct to within ±0°5, the principal source of error being drift of the incoming beam.

No dependence of polarization on sample orientation is seen in Table II, except for the MgO plate measurements (discussed in Sec. III A). A rigorous check is in Table II on fairy-castle layers Nos. 3 and 2, for which orientation comparisons were made at several phase angles. To eliminate possible time dependent effects, only orientation comparisons made on the same date will be considered. Five such comparisons at four phase angles (11°, 17°, 25°, 50°) are available for each of the two samples; all but one are with the *U* filter. The maximum difference between orientations *A* and *B* is 0.09% in *P* and 11°9 in θ_r (these occur at 25° phase where *P* is less than 1%). The algebraic averages are

0.016% and 0°35, which are much less than the probable errors discussed above. Comparisons are also available between orientations *B* and *D* for the solid lava fragment, using a nearly unpolarized tungsten light source on 9 September, namely for *G_u* at phases 11°, 17°, 25°, and 50°. The maximum differences are 0.73% and 19°7; the algebraic averages are 0.22% and 3°6. Again, no dependence on sample orientation is concluded, considering the small number of observations and the large scatter for this sample (which may have been caused by the use of a diaphragm too small compared to the scale of the irregularities of this fragment).

TABLE III. Angles of incidence for four orientations, *A-D*, of the samples.^a

Phase	<i>A</i>	<i>B</i>	<i>C</i>	<i>D</i>
0°0	-69°3	+45°0	-60°0	+ 0°0
11.0	-62.3	46.1	-49.0	11.0
17.0	-58.9	47.5	-43.0	17.0
25.0	-54.6	50.2	-35.0	25.0
50.0	-45.9	+63.0	-10.0	+50.0
90.0	+52.3	...	+30.0	...
110.0	+62.9	...	+50.0	...
135.0	+79.5	...	+75.0	...

^a The sample orientations are described in Sec. III B.

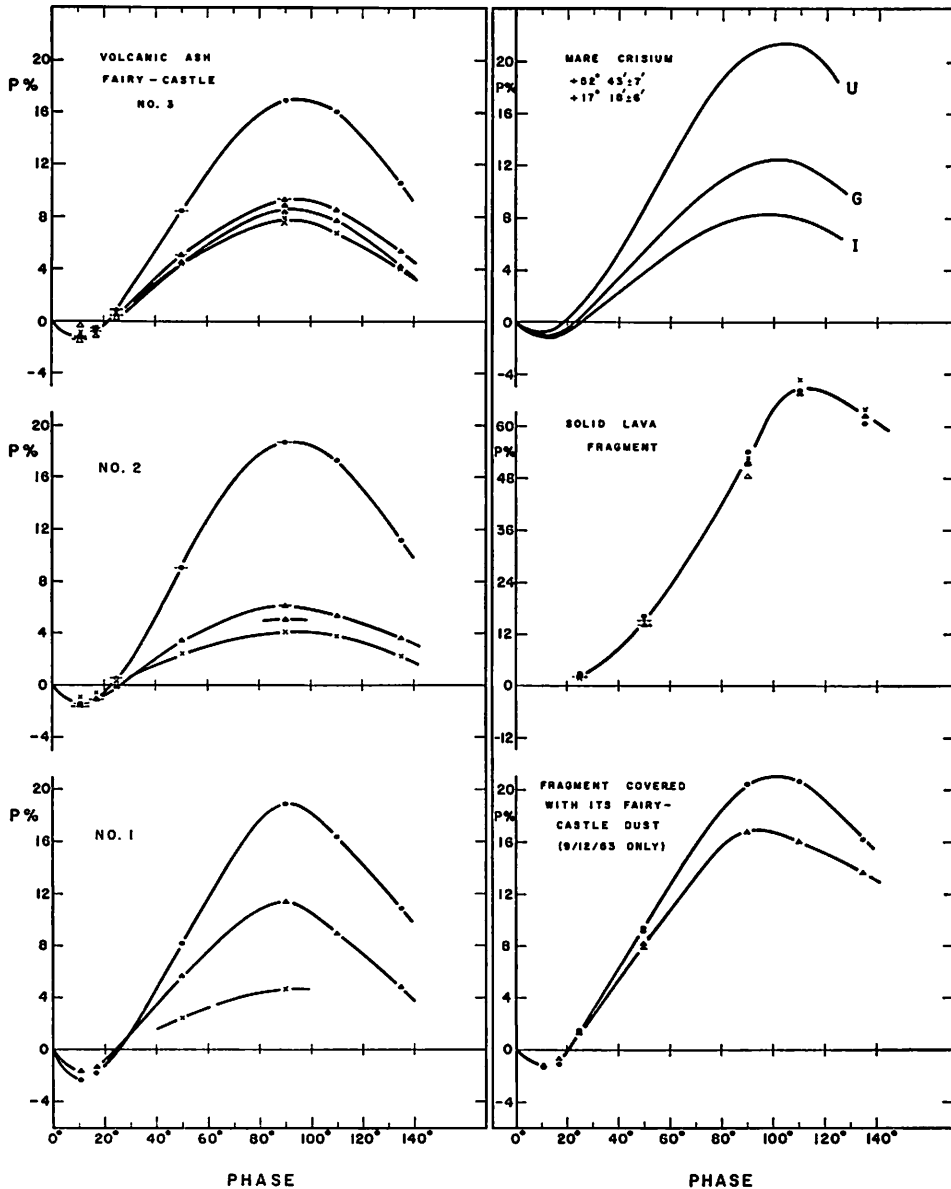


FIG. 2. The percentage polarization as a function of phase, observed with filters having effective wavelengths near 3600 \AA (filled circles), 5100 \AA (filled triangles), 5400 \AA (open triangles), and 9700 \AA (crosses). Short horizontal lines indicate multiple points. The curves for Mare Crisium are taken from Paper III; they are for Ultraviolet, Green, and Infrared filters, corresponding to U , G , and I in this paper.

c. Wavelength and Phase Dependence

Figure 2 shows the polarization data for the volcanic samples, with the exception of the following measurements:

(1) all wavelengths at 11° and 17° phase for the solid fragment, and a U value at 17° phase and a G_u value at 25° phase for fairy-castle No. 1, due to ambiguity in the sign of P (P is considered positive for $\theta \cong 180^\circ$, negative for $\theta \cong 90^\circ$).

(2) all September 15 measurements of the dust-covered lava fragment. This was a very delicate sample

since the dust was sifted onto the horizontal surface of the fragment. The fragment was subsequently tilted 45° for measurement, causing some of the very irregular dust-laden surfaces actually to overhang their dust layers. Any slight jarring caused some such dust to fall, thereby affecting the polarization properties. It is noted that the polarization of the solid fragment decreased by about three times when covered with dust. In Table II it is seen that the polarization increased markedly from 12 September to 15 September. Thus only the measurements of 12 September have been plotted—hopefully there was no appreciable change P during the 3-hour measuring run on that day.

On the whole the fairy-castle polarization is very similar to that of lunar regions. Curves for a small region in Mare Crisium are also given in Fig. 2 (Paper III). The inversion angle between 20° and 25° phase, and the phase of maximum polarization, are about the same for all four fairy-castle layers and for the moon. All plots in Fig. 2 are on the same scale except the solid lava fragment which is at $\frac{1}{3}$ scale. The solid fragment has three times the lunar polarization in the ultraviolet, it may or may not have a negative branch near zero phase, and it has little if any wavelength dependence.

Figure 3 gives the wavelength dependence for observations near 90° phase; it also includes Mare Imbrium and the terra crater Nicolai. Figure 3 suggests two types of wavelength dependence, namely, with and without the sharp bend near the green. It appears that the polarimetry of a fairy-castle structure composed of a mixture of lavas Nos. 1 and 3 is similar to that of Mare Crisium.

Only the solid lava fragment shows a definite increase of the phase of maximum polarization with decreasing wavelength (as found on the moon), though more observations near 90° phase are necessary to determine small differences.

The limited measurements of fairy-castle structures made from crushed charcoal and from crushed instant-tea particles (Table II), compared with those of crushed lava, demonstrate that the polarization is strongly dependent on the characteristics of the particles themselves, exclusive of the geometrical structure of the layer of particles. Note the extreme wavelength dependence at 90° phase for these particles.

4. Photometry

UGI differential photometry using a smoked MgO plate as comparison was done for the five samples, in orientation *B* (and sometimes *D*), at phases 0°, 11°, 17°, 25°, and 50°. Both phototubes of the Wollaston photometer were used with the Wollaston prism in a fixed orientation, with photometer depolarizer *in* the beam, and with a Lyot depolarizer between coelostat and sample.

The MgO standard was made by holding an aluminum plate over burning magnesium ribbon until a more-than-opaque layer was built up. This readily produces a sturdy MgO layer which is delicate only to actual contact. Three such plates were used, and a check showed their reflectivities to be within 0.01 mag. of each other in the ultraviolet and 0.02 mag. in the green.

a. Measurement and Reduction Procedures

The orientation of the MgO plate was always the same as that of the sample. The MgO plate could be set on the sample mount immediately in front of the sample,

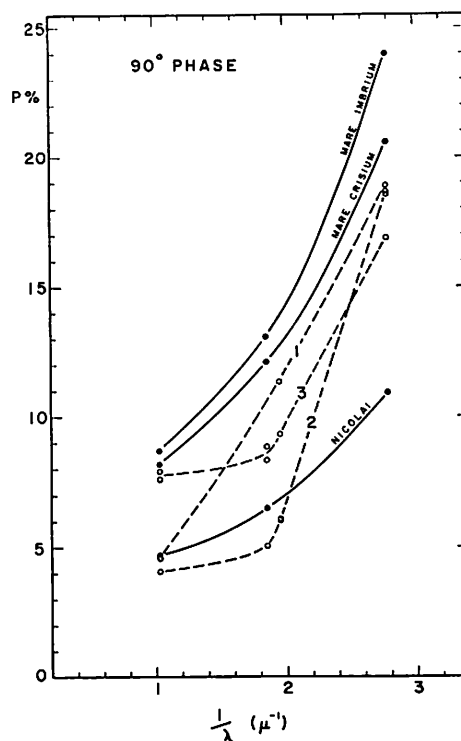


FIG. 3. The percentage polarization at 90° phase plotted as a function of the reciprocal of the wavelength in microns. The dashed curves are for various volcanic cinder fairy-castle structures (numbered in Sec. II). The solid curves for lunar regions are taken from Paper III.

and measurements (with usually a 20 sec integration time) were made in the sequence MgO-sample-MgO-sample-MgO. The drift of the image from the coelostat, variations in sky transmission, and the varied reflectivity of different parts of the mirrors caused some variation in the source intensity during a given sequence. For each sequence the average brightness difference between the sample and the MgO was obtained by averaging several readings. Readings were made, as for the polarimetry, with a magnitude ruler on the chart of the Brown recorder. The average of the readings of the two phototubes in the Wollaston photometer was always used. Graphical interpolation made possible an estimate of the sample brightness *during* the MgO integration, and vice versa.

Table IV lists magnitude differences under (*L-M*), that is *Lava-MgO*. The probable error is estimated to be ± 0.03 mag. on the basis of several repeated measurements and a consideration of the reduction procedure.

It is necessary to refer the brightness of the MgO plate at each orientation and phase angle to some standard orientation and phase, which was chosen to be at orientation *D* at 0° phase (i.e., perpendicular to both the incoming beam and the photometer). The transfers were made in two steps, as follows:

I. The brightness of the MgO plate at a given phase depends on its orientation. Therefore, comparisons of

TABLE IV. Magnitude differences of laboratory samples L with respect to a MgO plate M ; and to MgO plate at zero phase and normal incidence M_0 . Colors ($U-G$) and ($G-I$) relative to the MgO plate.

Sample	Phase	Filter ^a	($L-M$)	($L-M_0$)	Date 1963	($U-G$)	($G-I$)	
Volcanic ash; fairy-castle layer No. 3 (orientation B)	0°0	U	2 ^m 50	2 ^m 95	9/1	0 ^m 64	0 ^m 18	
		G_u	1.89	2.31	9/1			
		G_i	1.89	2.31	8/28			
		I	1.65	2.13	8/28			
	11.0	U	2.90	3.38	8/26	0.78	0.19	
		G_i	2.09	2.54	8/27			
		G_i	2.16	2.61	8/27			
		I	1.89	2.41	8/27			
	17.0	U	3.11	3.64	8/26	0.89	0.28	
		G_i	2.26	2.75	8/27			
		I	1.91	2.47	8/27			
	25.0	U	3.22	3.81	8/26	0.95	0.29	
		G_i	2.30	2.86	8/27			
		I	1.94	2.57	8/27			
	50.0	U	3.11	4.14	8/26 ^b	0.98	0.31	
U		3.28	4.31	8/26				
G_i		2.33	3.33	8/27				
I		1.96	3.02	8/27				
Volcanic ash; fairy-castle layer No. 2 (orientation B)	0°0	U	2.89	3.34	9/1	1.37	0.49	
		G_i	1.55	1.97	8/28			
		I	1.00	1.48	8/28			
	11.0	U	3.48	3.96	8/26	1.61	0.67	
		G_i	1.90	2.35	8/28			
		I	1.16	1.68	8/28			
	17.0	U	3.57	4.10	8/26	1.76	0.63	
		G_i	1.85	2.34	8/28			
		I	1.15	1.71	8/28			
	25.0	U	3.72	4.31	8/26	1.84	0.66	
		G_i	1.91	2.47	8/28			
		I	1.18	1.81	8/28			
	50.0	U	3.90	4.93	8/26	1.84	0.78	
		G_i	2.09	3.09	8/28			
		I	1.25	2.31	8/28			
Volcanic ash; fairy-castle layer No. 1 (orientation B)	11.0	U	3.14	3.62	9/14	0.88		
		G_u	2.29	2.74	9/14			
	17.0	U	3.28	3.81	9/14	0.94		
		G_u	2.38	2.87	9/14			
	25.0	U	3.43	4.02	9/14	0.95		
		G_u	2.51	3.07	9/14			
50.0	U	3.61	4.64	9/14	1.04	1.31		
	G_u	2.60	3.60	9/14				
	I	1.23	2.29	9/15				
Solid lava fragment (orientation D)	0.0	U	3.44	3.44	9/6	0.22		
		G_u	3.22	3.22	9/6			
	11.0	U	3.75	3.78	9/6	0.37		
		G_u	3.38	3.41	9/6			
	17.0	U	3.80	3.88	9/6	0.26		
		G_u	3.54	3.62	9/6			
	25.0	U	3.88	4.03	9/6	0.32		
		G_u	3.56	3.71	9/6			
	50.0	U	3.90	4.48	9/6	0.25		
		G_u	3.65	4.23	9/6			
	Solid lava fragment overlaid by its fairy-castle dust layer (orien- tation B)	0.0	I	2.85	3.33	9/15		
		11.0	U	2.97	3.45	9/12	0.32	
U			2.98	3.46	9/12			
G_u			2.71	3.16	9/12			
G_u			2.66	3.11	9/12			
17.0		U	3.11	3.64	9/12	0.40		
		G_u	2.75	3.24	9/12			
25.0		U	3.27	3.86	9/12	0.41		
		G_u	2.89	3.45	9/12			
50.0		U	3.56	4.59	9/12	0.40		
		G_u	3.19	4.19	9/12			

^a The filters are described in Table I.^b Orientation A . Sample orientations are described in Sec. III B.

orientations *B*, *D*, defined in Sec. III B, and *S* (*S* is with the MgO plate perpendicular to the direction to the Source) were made at each phase angle in the sequence *D*, *S*, *B*, *B*, *S*, *D*. These are plotted in Fig. 4 as differences (*B*−*S*) and (*D*−*S*), in magnitudes, for each filter (“*G*” is actually *G_u*, but also applies to *G_i*, within ±0^m.01). Incidentally, the curve of (*D*−*S*) seems wavelength-independent, whereas the (*B*−*S*) curves show a dependence in the order *G*, *U*, *I*. The transfer values were read from the smooth curves and are correct to within ±0.01 mag. (p.e.).

II. The brightness-phase dependence of the MgO plate was measured with the plate in orientation *D* (perpendicular to the photometer). This was done at all wavelengths but only for the *U* filter is the phase function well-defined (Fig. 5); the difficulty was in the variation of the incident light intensity during the minutes spent moving the photometer to different phase-angle positions. The points in Fig. 5 are numbered in the sequence of measurement (11°, 17°, 25°, 50°, 50°, 25°, 17°, 11°); apparently the intensity steadily increased during the sequence. The zero-phase point was obtained by extrapolation of a cosine-curve fit. The

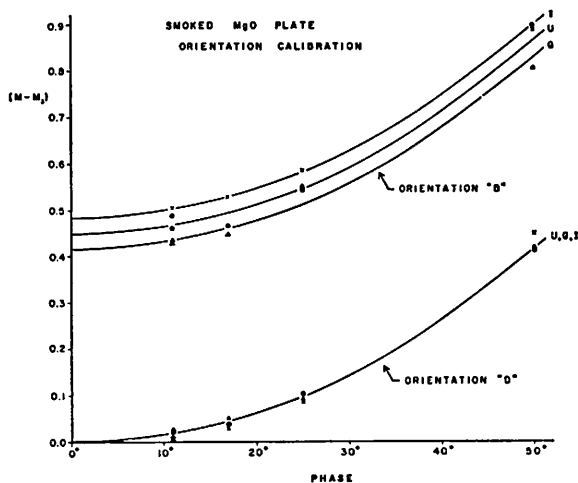


FIG. 4. Magnitude differences between orientation *B* (and *D*) and orientation *S* (perpendicular to the source) plotted as a function of the phase angle, for the MgO comparison plate. The filter symbols are as in Fig. 2.

complexities in the transfer to the standard position, the direct (*L*−*M*) measures are also listed in Table IV.

b. Colors

The last two columns of Table IV list the *UGI* colors of the samples relative to the color of sunlight reflected from the MgO plate, at each phase angle. Stebbins and Kron (1957) found that a similarly smoked MgO disk (in combination with an aluminized sphere and a quartz lens) produced no color deviations greater than ±0.03 mag. The colors in Table IV therefore are approximately those relative to sunlight. Following Kron (1963) the sun has (*U*−*G*) = −0.11 mag. and (*G*−*I*) = −0.20 mag.

Table V gives the resulting sample colors in the Stebbins-Whitford *UGI* system (obtained from the measurements in the present *UG_uG_iI* system by

TABLE V. *U*, *G*, *I* colors.

Object	0° Phase		50° Phase	
	<i>G</i> − <i>I</i>	<i>U</i> − <i>G</i>	<i>G</i> − <i>I</i>	<i>U</i> − <i>G</i>
Fairy-castle layer No. 1	+0 ^m .73	+1 ^m .31
Fairy-castle layer No. 2	+0 ^m .17	+1 ^m .43	+0.40	+1.97
Fairy-castle layer No. 3	−0.08	+0.62	+0.04	+0.98
Solid fragment	...	+0.18	...	+0.23
Solid fragment with dust	+0.42
Whole moon	+0.20	+0.47	+0.31	+0.69

magnitude differences between the values at each phase and at zero phase are +0.03 (11°), +0.08 (17°), +0.15 (25°), and +0.58 mag. (50°), with a probable error of about ±0.01 mag. Plotted on an intensity scale this phase function differs slightly from a cosine curve (less than 5% at 50° phase, when normalized to 11° phase), in that the intensity drops off more rapidly with increasing phase than does the cosine curve. The phase function of Fig. 5 was also used for *G* and *I* values; various measurements with these filters indicate that this is a fair approximation (within 0.05 mag.).

The only sample-orientation transfers necessary for the reductions are (*B*−*D*) magnitude differences, which are constant with phase (as seen by the constant separations between the curves in Fig. 5); the following values were applied: +0.45 (*U*), +0.42 (*G*), and +0.48 mag. (*I*). The values (*L*−*M₀*) of the difference between the sample, and the MgO plate at zero phase and orientation *D*, given in Table IV, were formed by adding the appropriate orientation and phase transfers to the (*L*−*M*) values. The probable error of the (*L*−*M₀*) values is about ±0.03 mag. Because of the

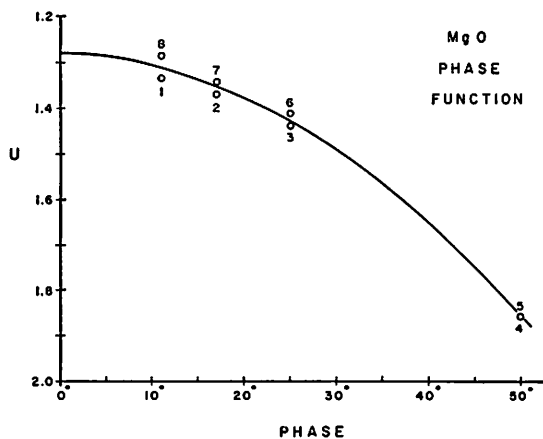


FIG. 5. Ultraviolet magnitudes of the MgO plate in orientation *D* as a function of phase angle. The points are numbered in the sequence of measurement.

graphical interpolation to UGI wavelengths—the maximum difference between corresponding wavenumbers of the two systems is $\pm 0.21 \mu^{-1}$). The UGI colors of the whole moon are taken from Paper III. The probable errors of the values in Table V are approximately ± 0.05 mag. The $(G-I)$ color of fairy-castle layer No. 2 is similar to that of the moon, but all of the fairy-castle layers are redder than the moon in $(U-G)$.

c. Phase Dependence

Figure 6 shows on the left the magnitude-phase relations in the ultraviolet, and on the right the color-phase relations. The magnitude-phase relations are in terms of $(L-M_0)$, which is the difference, in magnitudes, between the brightness of the sample and the brightness of the magnesium oxide plate, the latter at zero phase and normal incidence (Sec. IV A). An ultraviolet opposition effect (that is, a surge of brightness near zero phase) is exhibited by the three samples which were measured at 0° phase; it is more pronounced for fairy castles than for the solid lava fragment. But little opposition effect is present in the green or infrared. Consequently, the fairy-castle structures show a pronounced increase in $(U-G)$ with increasing phase. The solid lava fragment has little if any $(U-G)$

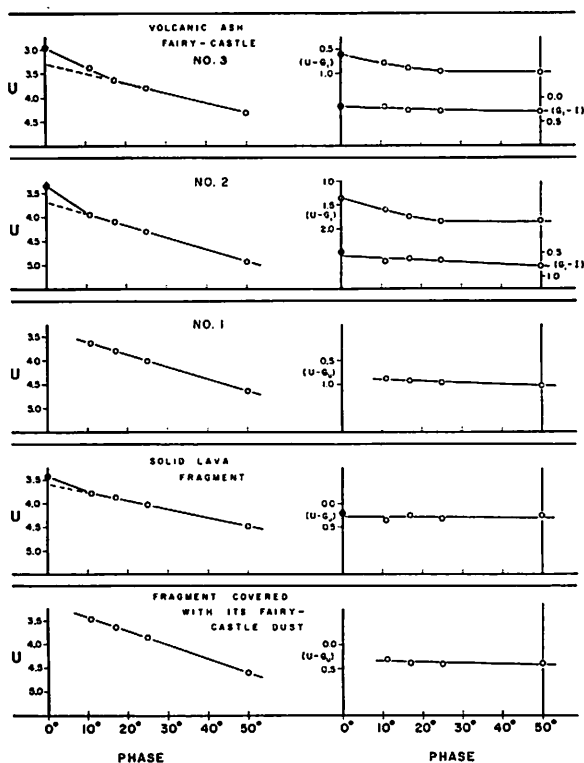


FIG. 6. On the left, ultraviolet magnitude differences (sample minus MgO plate in standard position) as a function of phase. On the right, UGI magnitude colors as a function of phase; the subscripts i and u indicate the phototubes that were used, as described in Table I.

color-phase effect. At phases greater than 20° , the magnitude-phase functions are all approximately linear.

Table VI gives the slopes of the ultraviolet magnitudes between phases 20° and 50° , and also the zero-phase excesses compared to the extrapolations of the linear portions (i.e., measures of the opposition effect).

5. Concluding Remarks

An exact fit to the lunar observations has not yet been obtained in the laboratory. The opposition effect is present on the moon at all UGI wavelengths, and the lunar nonlinearity is confined to phases less than about 5° .

A particulate texture gives about the same polarization-wavelength dependence as that of the lunar surface. The amounts of polarization and brightness in the visual region can also be reproduced in the laboratory as shown by Hapke (1964a). This study by Hapke indicates that solar-wind bombardment can appreciably modify the photometry and polarimetry of various materials; proton bombardment of dielectric powders invariably lowers the albedo, sharpens the brightness backscatter peak, and increases the polarization at all phase angles. Consequently it is probably unrealistic to search for an unbombarded sample which reproduces the lunar polarization. But the increase in P by bombardment might be offset by a decrease in P brought about by a decrease in the particle sizes used for the fairy-castle structures. Hapke (1964b) finds that P_{max} decreases rapidly as the particle diameter decreases from 100 to 10μ , and also as the degree of compaction of the dust layer decreases.

Gehrels *et al.* (Paper III) conclude a lunar surface composed of a thin partially transparent cloud of repelling particles with diameters of the order of 1.6μ , overlying a more compacted surface. The lunar

TABLE VI. Photometric phase factors and opposition effects.

Sample	Phase factor $20^\circ < a < 50^\circ$ (mag./deg)			Excess at zero phase		
	U	G	I	U	G	I
Fairy-castle layer No. 1	0^m026	0^m022^b
Fairy-castle layer No. 2	0.025	0.022^a	0.018	0^m36	0^m00	-0^m03
Fairy-castle layer No. 3	0.015	0.018^a	0.017	0.36	0.12	+0.03
Solid fragment	0.018	0.020^b	...	0.16	0.01	...
Solid fragment with dust	0.029	0.028^b
Whole moon ^c	0.033	0.029^a	0.026	0.53	0.51	+0.50

^a G_i .

^b G_u . The difference between G_i and G_u is shown in Table I.

^c Approximate values taken from Paper III.

polarimetry can probably be reproduced by a layer of particles having the right balance of particle diameter, compaction, bombardment, and perhaps contribution of higher polarization from an underlying surface, although the effect of these parameters on the *wavelength* dependence is largely unknown.

In conclusion, the author wishes to acknowledge the interdepartmental cooperation at the University of Arizona for this work. The study was a part of a joint polarimetry program of the Institute of Atmospheric Physics and the Lunar and Planetary Laboratory. The Astronomy Department provided the theodolite and other facilities, and the Physics Department made laboratory space available. The author is most grateful to Dr. T. Gehrels for his guidance and suggestion of this research.

This work was supported by the Office of Naval Research.

REFERENCES

- Bumba, V., Topolová-Růžičková, B. 1962, *Bull. Astron. Inst. Czech.* 13, 95.
- Gehrels, T., Coffeen, T., and Owings, D. 1964, *Astron. J.* 69, 826 (Paper III).
- Gehrels, T., and Teska, T. M. 1960, *Publ. Astron. Soc. Pacific* 72, 115.
- . 1963, *Appl. Opt.* 2, 67.
- Hapke, B. 1964a, Center for Radiophysics and Space Research, Rept. No. 169, Cornell University, Ithaca, New York.
- . 1964b, "Photometric and Other Laboratory Studies Relating to the Lunar Surface," *The Lunar Surface Layer*, edited by Salisbury and Glaser (Academic Press Inc., New York).
- Hapke, B., and Van Horn, H. 1963, *J. Geophys. Res.* 68, 4545.
- Kron, G. E. 1963, *Publ. Astron. Soc. Pacific* 75, 288.
- Liot, B. 1929, *Ann. Obs. Meudon*, 8; also in *Tech. Transl. F-187* (National Aeronautics and Space Administration, Washington, D. C. 1964).
- Stebbins, J., and Kron, G. E. 1957, *Astrophys. J.* 126, 266.

TABLE OF CONTENTS

No. 64	The Composition of the Surface Layer of Mars..... by Alan B. Binder and Dale P. Cruikshank	111
No. 65	Martian Cratering..... by William K. Hartmann	121
No. 66	Preliminary Drawings of Lunar Limb Areas, VI..... by Alike K. Herring	133
No. 67	Observations of Comet Ikeya-Seki (1965f) from Mauna Kea, Hawaii..... by Alike K. Herring	141
No. 68	Observations of Comet Ikeya-Seki (1965f) from Tucson, Arizona..... by Stephen M. Larson	145
No. 69	Wavelength Dependence of Polarization, IV: Volcanic Cinders and Particles..... by David L. Coffeen	157